Renewable Energy 170 (2021) 327–340

Contents lists available at ScienceDirect

Renewable Energy

journal homepage: www.elsevier.com/locate/renene

A novel parabolic trough receiver by inserting an inner tube with a wing-like fringe for solar cascade heat collection☆

Peng Liu , Zhimin Dong , Hui Xiao , Zhichun Liu , Wei Liu *

School of Energy and Power Engineering, Huazhong University of Science and Technology, Wuhan, 430074, PR China

ARTICLE INFO

Article history:
Received 4 December 2020
Received in revised form
18 January 2021
Accepted 29 January 2021
Available online 2 February 2021

Keywords:
Solar cascade heat collection
Novel parabolic trough receiver
Inner tube
Wing-like fringe
Overall efficiency

ABSTRACT

In this work, a novel parabolic trough receiver (NPTR) with an inner tube and wing-like fringe was proposed to improve heat-collecting efficiency as well as provide different grades of thermal energy. Thermal oil and water, which flow respectively in absorber and the inner tube, are selected as high and low temperature heat transfer fluids. A three-dimensional computational fluid dynamics model was developed to investigate the performance of the NPTR. Effects of geometrical parameter and thermal conductivity of inner tube on the performance of NPTR were studied in details. Based on the results, the NPTR with $\beta = 180^{\circ}$ is recommended as the suggested design. Moreover, performance of the suggested design under different direct normal irradiances (300−1000 W/m^2) and inlet temperature of oil (400 −650 K) were evaluated. Compared to the conventional parabolic trough receiver, the heat loss of NPTR is effectively reduced by 33.1−50.1%, and the overall efficiency can be improved by 0.61%−7.67%. Moreover, the proportions of oil and water heat gains in the total input solar energy are ranged in −18.8−63.5% and 8.39−77.6%, and the temperature gains of oil and water are ranged in −1.4−19.5 K and 5.4−18.8 K, respectively.

1. Introduction

Fossil fuels, the main energy sources for the development of the world, are being consumed rapidly with the booming development of the world economy [1]. The problems that come along, including energy shortage, environmental pollution, global warming from greenhouse effect and so on, are becoming increasingly serious [2]. Speeding up the development and utilization of clean and renewable energy is an effective way to alleviate these problems. Solar energy, the world's most abundant clean energy source, has great potential to partially replace fossil energy and meet the growing energy demand [3]. Photothermal and photovoltaics are the two main ways of solar energy utilization [4]. Among them, solar thermal utilization can provide the required heat source for production and living processes, such as concentrating solar power (CSP) [5], solar-powered desalination [6,7], solar water heater [8], and so on. Parabolic trough collector (PTC), the most mature concentrating solar thermal collector, is the most widely used collector in CSP stations and contributes over 75% to the global CSP capacity [9]. Thus, the design and research on the PTC have drawn extensive attention from researchers all over the world [10,11].

The PTC is composed of a reflector and a parabolic trough receiver (PTR) that consists of an absorber, glass cover and annular vacuum zone between them. When the PTC is working, the upper half part of the absorber receives direct irradiance while the lower half part receives concentrated irradiance from the reflector (see Fig. 1(b)). The solar irradiance will be absorbed by the selective coating on the outer surface of the absorber and then converted to a non-uniform heat flux. Finally, most of the heat will be taken away by the heat transfer fluid (HTF) in the absorber. Part of the heat will be lost to the environment through the radiative heat transfer between the absorber outer surface and inner wall of glass cover and then the radiative and convective heat transfer on the outer wall of glass cover. And the heat loss will increase rapidly with the increasing temperature of HTF in a conventional parabolic trough receiver (CPTR). Thus, the key to reducing heat loss is how to shrink the heat transfer between the absorber outer surface and inner wall of glass cover. To improve the efficiency and competitiveness of PTC, researchers all over the world have made a great amount of

☆ Present Address: School of Energy and Power Engineering, Huazhong University of Science and Technology, Wuhan, 430074, P.R. China.
* Corresponding author.
E-mail addresses: peng_liu@hust.edu.cn (P. Liu), dongzhimin@hust.edu.cn (Z. Dong), xiaohui_hust@foxmail.com (H. Xiao), zcliu@hust.edu.cn (Z. Liu), w_liu@hust.edu.cn (W. Liu).

https://doi.org/10.1016/j.renene.2021.01.138
0960-1481/

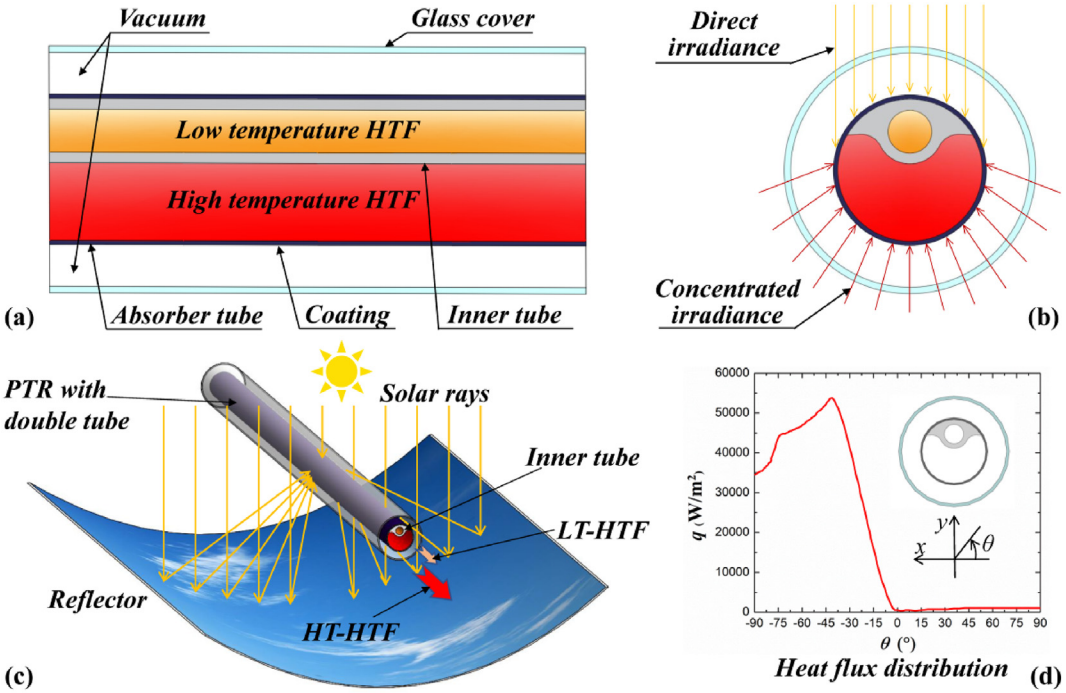

Fig. 1. Sketch of a novel PTR inserted by an inner tube with a wing-like fringe.

efforts to reduce its heat loss [3,10]. Until now, a variety of technologies have been proposed, including heat loss lessening technologies that focus on the radiative heat transfer between absorber and glass cover, and the heat transfer enhancement technologies that focus on the flow and heat transfer of HTF within absorber.

Heat loss lessening technologies are aimed at hindering the radiative heat transfer between the absorber outer surface and inner wall of glass cover, such as adding radiation shield [12,13], adding transparent aerogel [14,15], etc. Yang et al. [16] have conducted a spectral-spatial design and coupling analysis of a PTR under the HTF temperature of 600 °C. They found that over 40% surface area of the absorber (mainly in the directly illumined zone) is the negative thermal-flux region, which means that the radiative heat flux density from absorber to the environment exceeds the direct solar irradiance when the PTR is working under a high HTF's temperature. To overcome the negative thermal-flux region, Wang et al. [17] have designed, manufactured and tested a PTR with a radiation shield that made of aluminum. They found that the heat loss can been effectively reduced up to 28.1% when at the absorber temperature of 600 °C and the efficiency are significantly enhanced by 12.9% when DNI is 600 W/m^2 and inlet temperature is 550 °C. However, because the radiation shield inevitably intercepts part of the direct irradiance, the results indicated that the heat-collecting efficiency of the PTR with shield is even lower than that of a CPTR when the temperature of HTF is low and the DNI is large. Li et al. [14] and Qiu et al. [15] have proposed an excellent strategy by adding solar-transparent aerogel in the directly illumined vacuum zone. The solar-transparent aerogel possesses an outstanding solar transmittance and but low transmittance to infrared emittance. They found that this design can alleviate the optical blocking by the radiation shield and effectively improve the efficiency of PTR under large range of DNI and HTF's temperature. Recently, Qiu et al. [18] have designed a novel PTR with a spectral-selective glass cover and rabbit-ear mirrors and obtained a maximum receiver efficiency improvement of 2.72%.

Heat transfer enhancement technologies and theories [19,20], which are often applied to enhance the heat or mass transfer between the fluid and solid, have been widely studied for reducing the temperature of absorber and improving performance of PTR, including nanofluids and turbulators. Among them, nanofluids are still far away from large-scale industrial applications due to their high production cost, agglomeration and instability [21,22]. While turbulators, which focus on disturbing and promoting the mixing of the HTF so as to enhance the heat transfer, have good potential in practical applications due to their low cost, easy manufacture and installation [23,24]. In recent years, various turbulators have been proposed for improving the performance of PTR, such as twisted tape [25], helical screw tape [26], conical strip [27], porous disc [28], rod [29], perforated plate [30], metal foams [31], internal fin [32,33], longitudinal vortex generators [34], inclined curved-twisted baffles [35], ribbed tube [36], corrugated tube [37], etc. Mwesigye et al. [30] have examined the performance of a PTR with centrally placed perforated plate inserts. It was found that the perforated plate can improve the thermal efficiency by 1.2–8%. Bellos et al. [38] employed a internally finned absorbers to ameliorate the performance of the PTR and obtained 1.27% increase in the thermal efficiency at inlet HTF temperature of 600 K. Liu et al. [27] reported a numerical study of a PTR with conical strip inserts. They found that the enhanced PTR can obtain up to 82.1% reduction in heat loss and 5.04% enhancement in thermal efficiency. However, the performance enhancement of the PTR with turbulators is limited when the when the temperature and flow rate of HTF are high and the DNI is low. It is because that under this condition, it is difficult for the PTR with turbulators to achieve obvious reduction in temperature on the absorber outer surface compared to the CPTR. Moreover, the turbulators are unable to overcome the negative thermal-flux region in the directly illumined zone.

As the global water shortage is getting worse, desalination technologies driven by solar energy for clean fresh water production have drawn extensively interests around the world recently [39–43]. Desalination technologies such as multi-effect membrane distillation [42] require a great amount of low-grade heat (about 80 °C) which can be provided by solar thermal collectors. In some arid regions with abundant solar energy resources like North Africa, the Middle

East and some remote islands, etc., solar energy has potential to meet the demands of energy for electricity and fresh water production. This requires solar collectors to provide high temperature and low temperature heat sources for power production and water desalination at the same time. Recently, Liu et al. [44] designed a novel PTR with double tube for solar cascade heat collection and numerically investigated the effects of the operating parameters on the performance. They found that the proportions of the high and low temperature heat gains are ranged in 39.01–62.92% and 28.37–8.86% of the incident solar energy, respectively and the total thermal efficiency can be improved by up to 1.5%.

Based on the literature survey above, to overcome the negative thermal-flux region and improve heat-collecting efficiency as well as provide different grades of thermal energy, a novel parabolic trough receiver (NPTR) by integrating an inner tube with a wing-like fringe for solar cascade heat collection is designed, as shown in Fig. 1. In the NPTR, an inner tube with a wing-like fringe is tightly affixed to the upper half of absorber. Low temperature heat transfer fluid (LT-HTF) such as seawater or brine in the inner tube, which is used to provide low-grade thermal energy for desalination, can take away the heat from direct irradiance and effectively reduce the temperature and heat loss in the directly illumined zone of absorber. At the same time, the high temperature heat transfer fluid (HT-HTF), which flows between the inner tube and absorber inner surface, can take away the heat from concentrated irradiance and provide high-grade thermal energy for power production. In the present work, firstly, a three-dimensional numerical model is established for evaluating the performance of the NPTR. Then, the effects of geometrical and thermal-physical property parameters of the inner tube on the performance are investigated. Finally, performance of the NPTR under different DNI is studied and evaluated. This study may provide an alternative efficient solar heat collector for the cascade comprehensive utilization of solar thermal energy.

2. Description of the novel parabolic trough receiver

The novel parabolic trough receiver (NPTR) proposed in this study is modified from a standard LS2 PTC [26] by integrating an inner tube with a wing-like fringe, as shown in Fig. 1. And the geometric model of the NPTR is presented in Fig. 2. The detailed geometrical and thermal parameters of the NPTR are listed in Table 1. To obtain both high and low temperature heat sources for power generation and desalination, respectively, two heat transfer fluids (HTFs), i.e. high temperature heat transfer fluid (HT-HTF) and low temperature heat transfer fluid (LT-HTF), are applied in the NPTR, as shown in Fig. 1. Moreover, the LT-HTF flows through the inner tube while the HT-HTF flows through the channel between the inner surface of absorber and the inner tube. Syltherm-800 oil [45] and water are selected as the HT-HTF and LT-HTF in this study, respectively.

Because the heat loss is mainly through the radiation heat exchange between the outer surface of absorber and the glass cover and then is lost to the environment. Reducing the temperature of the absorber will be an effective way to diminish the heat loss according to Stefan-Boltzmann law. Therefore, the inner tube in this study is designed to be tightly affixed to the upper half of absorber, where is illuminated by direct solar irradiance and loaded with low heat flux density, as shown in Fig. 1. The LT-HTF goes through the inner tube and takes away the heat and the wing-like fringe of the inner tube can prevent the HT-HTF from directly contacting the upper part of absorber. The combination of these two strategies makes it possible to maintain the upper part of absorber at a relatively lower temperature than that of the HT-HTF. In addition, six different central angles ($\beta = 60°, 90°, 120°, 150°, 180°$ and $210°$) corresponding to the wing-like fringe have been selected to determine its influence on the performance of the NPTR. The material of the inner tube should possess good resistance to the high temperature and seawater corrosion as well as excellent mechanical properties. Thus, zirconia ceramic become a good choice for the inner tube material. Moreover, the thermal conductivity of the inner tube should be low enough to minimize heat transfer from HT-HTF to LT-HTF. Therefore, porous zirconia ceramic [46] with thermal conductivity of 0.1–0.7 W/(m K) has been selected as the material of the inner tube. To explore the effects of the thermal conductivity of the inner tube on the performance of the NPTR, six different thermal conductivities ($\lambda_{innertube}$ = 0.2, 0.3, 0.4, 0.5, 0.6, 0.7 W/(m·K)) have been selected to be investigated in this study.

3. Numerical model

In the conventional parabolic trough receiver (CPTR), the pivotal flow and heat transfer processes include heat convection between the HT-HTF and the absorber inner surface, heat conduction within the absorber, glass cover and the vacuum domain, thermal radiation between the absorber and the glass cover, heat convection on the outer surface of glass cover with environment, and the thermal radiation between the outer surface of glass cover and sky. In the NPTR, the heat convection between inner tube and both HT-HTF and LH-HTF, heat conduction in the inner tube should be further considered. A three-dimensional computational fluid dynamics (CFD) model was established to simulate the flow and heat transfer processes mentioned above. In addition, considering that the NPTR is symmetry about the *x*-*z* plane, only half of the NPTR is selected as the computational domain to save computing resource.

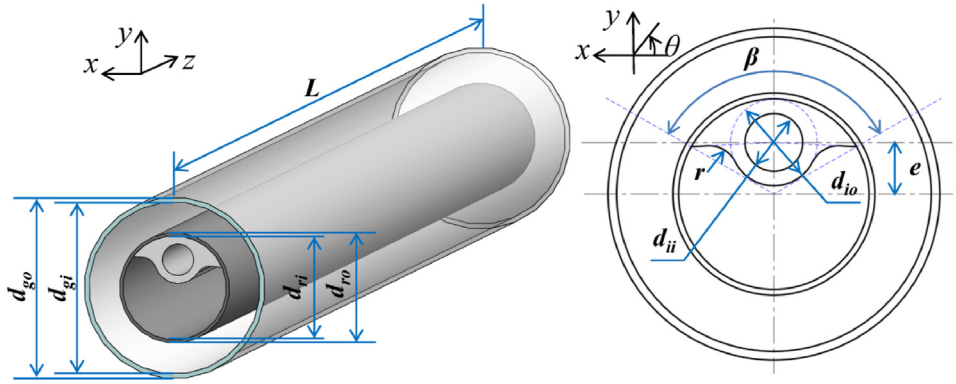

Fig. 2. Geometric models of the NPTR.

Table 1
Geometrical and thermal parameters of the NPTR [15,26,47].

Parameters	Value	Parameters	Value
Full length of the PTR (L)	7.8 m	Emissivity of the glass cover (ε_g) [15]	0.86
Inner diameter of absorber (d_{ri})	66 mm	Density of the glass cover	2230 kg/m^3
Outer diameter of absorber (d_{ro})	70 mm	Thermal conductivity of the glass cover [15]	1.2 W/(m·K)
Inner diameter of glass cover (d_{gi})	109 mm	Temperature-dependent emissivity selective coating (ε_c) [47]	0.000327 T −0.065971
Outer diameter of glass cover (d_{go})	115 mm	Density of absorber	7650 kg/m^3
Inner diameter of inner tube (d_{ii})	20 mm	Thermal conductivity of absorber [26]	25 W/(m·K)
Outer diameter of inner tube (d_{oi})	30 mm	Mass flow rate of Syltherm-800 oil	0.7 kg/s
Eccentric distance of inner tube (e)	18 mm	Mass flow rate of water	0.12 kg/s
Radius of rounded corners (r)	10 mm	Density of inner tube (zirconia ceramic)	5700 kg/m^3

3.1. Computational methods

In this study, the flow and heat transfer processes in the CPTR and NPTR are assumed to be in steady state. The flow of both HT-HTF and LT-HTF is assumed to be turbulent. The realizable k-ε two-equation turbulence model, which has been verified in our previous work [27], is adopted to simulate the flow and heat transfer of the HTFs, and the corresponding governing equations are expressed as below.

Continuity equation:

$$\frac{\partial(\rho u_i)}{\partial x_i}=0 \tag{1}$$

Momentum and energy equations for the HTFs:

$$\frac{\partial(\rho u_i u_j)}{\partial x_i}=-\frac{\partial P}{\partial x_i}+\frac{\partial}{\partial x_j}\left((\mu+\mu_t)\times\left(\frac{\partial u_i}{\partial x_j}+\frac{\partial u_j}{\partial x_i}\right)-\frac{2}{3}(\mu+\mu_t)\frac{\partial u_i}{\partial x_i}\delta_{ij}-\rho\overline{u_i' u_j'}\right) \tag{2}$$

$$\frac{\partial(\rho u_i T)}{\partial x_i}=\frac{\partial}{\partial x_i}\left(\frac{\mu}{\mathrm{Pr}}+\frac{\mu_t}{\mathrm{Pr}_t}\right)\frac{\partial T}{\partial x_i} \tag{3}$$

where μ_t and Pr_t are the turbulent viscosity and turbulent Prandtl number, respectively.

Equations of Turbulent kinetic energy k and turbulent energy dissipation ε:

$$\frac{\partial(\rho u_i k)}{\partial x_i}=\frac{\partial}{\partial x_i}\left(\left(\mu+\frac{\mu_t}{\sigma_k}\right)\frac{\partial k}{\partial x_i}\right)+\Gamma-\rho\varepsilon \tag{4}$$

$$\frac{\partial(\rho u_i \varepsilon)}{\partial x_i}=\frac{\partial}{\partial x_i}\left(\left(\mu+\frac{\mu_t}{\sigma_\varepsilon}\right)\frac{\partial \varepsilon}{\partial x_i}\right)+c_1\Gamma\varepsilon-\rho c_2\frac{\varepsilon^2}{k+\sqrt{\nu\varepsilon}} \tag{5}$$

$$\Gamma=-\overline{u_i u_j}\frac{\partial u_i}{\partial x_i}=\mu_t\left(\frac{\partial u_i}{\partial x_j}+\frac{\partial u_j}{\partial x_i}\right)\frac{\partial u_i}{\partial x_i} \tag{6}$$

where σ_k and σ_ε represent the turbulent Prandtl numbers for k *and* ε, respectively.

The energy equation for the heat conduction in the solids is presented as follow:

$$\frac{\partial}{\partial x_i}\left(\lambda\frac{\partial T}{\partial x_i}\right)+S_h=0 \tag{7}$$

where S_h is the heat source which equals to 0 in this study.

Software ANSYS Fluent 16.0 based on the finite volume method (FVM) is employed to solve all the governing equations. The governing equations are discretized with second order upwind scheme. The coupling between velocity and pressure is obtained with SIMPLE algorithm. In addition, the enhanced wall treatment method is employed to capture the high resolution of gradients near the surfaces. Discrete Ordinates (DO) radiation model is selected to simulate the radiative heat transfer.

The materials of the absorber and glass are stainless steel (321H) and Pyrex with the thermophysical properties listed in Table 1. The temperature-dependent thermophysical properties of the Syltherm-800 oil [45] are presented in Eqs. 8–11, while the temperature-dependent thermophysical properties of water, which are fitted into polynomials from the data in the reference [45], are expressed in Eq. 12–15, where T is the temperature of the HTFs in K.

$$\rho_{\mathrm{oil}}=-6.0616\times10^{-4}T^2-4.1535\times10^{-1}T+1.1057\times10^{3} \tag{8}$$

$$c_{p,\mathrm{oil}}=1.7080T+1.1078\times10^{3} \tag{9}$$

$$\lambda_{\mathrm{oil}}=-5.7534\times10^{-10}T^2-1.8752\times10^{-4}T+1.9002\times10^{-1} \tag{10}$$

$$\mu_{\mathrm{oil}}=6.6720\times10^{-13}T^4-1.5660\times10^{-9}T^3+1.3882\times10^{-6}T^2-5.5412\times10^{-4}T+8.4866\times10^{-2} \tag{11}$$

$$\rho_{\mathrm{water}}=1.772\times10^{-5}T^3-2.067\times10^{-2}T^2+7.335T+1.71956\times10^{2} \tag{12}$$

$$c_{p,\mathrm{water}}=1.471\times10^{-6}T^4-1.973\times10^{-3}T^3+1.005T^2-2.2965\times10^{2}T+2.3978\times10^{4} \tag{13}$$

$$\lambda_{\mathrm{water}}=3.419\times10^{-8}T^3-4.581\times10^{-5}T^2+2.014\times10^{-2}T-2.229 \tag{14}$$

$$\mu_{\mathrm{water}}=4.078\times10^{-11}T^4-5.502\times10^{-8}T^3+2.789\times10^{-5}T^2-6.302\times10^{-3}T+0.536574 \tag{15}$$

3.2. Boundary conditions

The detailed boundary conditions employed in the present work are listed as follows:

(1) No slip conditions were applied to the interfaces between the solids and HTFs.
(2) The HT-HTF and LT-HTF flow in the same direction (parallel flow). The mass flow rates of the HT-HTF and LT-HTF at the inlets were set to be 0.7 kg/s and 0.12 kg/s, respectively. Pressure outlets were employed to the outlets of the HTFs.
(3) A circumferential non-uniform heat flux distribution under direct normal irradiance (DNI) of 1000 W/m^2 from He's research [48], as shown in Fig. 1 (d), was loaded on the outer surface of absorber. And the temperature-dependent emissivity selective coating [47], which is listed in Table 1, was employed at the absorber outer surface.
(4) The surfaces of the glass cover and absorber were assumed to be opaque and gray to the infrared radiation. The emissivity on surfaces of the glass cover is set to 0.86 [15].
(5) Adiabatic boundary was adopted to the ends of the receiver.
(6) At the outer surface of the glass cover, a mixed boundary of heat convection and radiation was applied. The heat transfer flux that lost to the environment was calculated by using the following equation:

$$q = h_w(T_w - T_a) + \varepsilon_g \sigma\left(T_w^4 - T_s^4\right) \tag{16}$$

where T_w is the temperature on the outer wall of the glass cover. T_a is the ambient temperature which equals to 298 K in this study, while T_s is the sky temperature which is 8 K lower than T_a [49]. σ is the Stefan-Boltzmann constant. ε_g is the emissivity of the glass. h_w is the approximate uniform convective heat transfer coefficient on the outer wall of the glass cover, which can be defined as Eq. (17) [50].

$$h_w = 4V_w^{0.58} d_{go}^{-0.42} \tag{17}$$

where V_w is the wind speed which is set to 2.5 m/s in this study.

3.3. Parameter definitions

The Reynolds number (Re), average heat transfer coefficient (h), average Nusselt number (Nu) and friction factor (f) are defined as below:

$$Re = \frac{\rho u d}{\mu} \tag{18}$$

$$h = q_w \Big/ \left(T_w - T_f\right) \tag{19}$$

$$Nu = hd/\lambda \tag{20}$$

$$f = \frac{2\Delta P_L d}{\rho u^2} \tag{21}$$

where ρ, μ and λ are the density, viscosity and thermal conductivity of the HTFs at T_f, respectively. q_w and T_w represent the average heat flux and temperature on the inner surface of absorber or inner tube, respectively. T_f and u are the bulk temperature average velocity of the HTFs, and d is the inner diameter of absorber or inner tube, and ΔP_L is the pressure drop per unit distance in the flow direction.

The heat gain (Q_u) and pumping work (W_p) of the HTFs are defined as follow:

$$Q_{u,oil} = M_{oil} \cdot c_{p,oil} \cdot \left(T_{out,oil} - T_{in,oil}\right) \tag{22}$$

$$Q_{u,water} = M_{water} \cdot c_{p,water} \cdot \left(T_{out,water} - T_{in,water}\right) \tag{23}$$

$$Q_u = Q_{u,oil} + Q_{u,water} \tag{24}$$

$$W_{p,oil} = M_{oil} \cdot \Delta P_{oil} \Big/ \rho_{oil} \tag{25}$$

$$W_{p,water} = M_{water} \cdot \Delta P_{water} / \rho_{water} \tag{26}$$

$$W_p = W_{p,oil} + W_{p,water} \tag{27}$$

The overall efficiency can be calculated as Eq. (28) [10] as below:

$$\eta = \frac{Q_u - W_p/\eta_{el}}{Q_s} \tag{28}$$

$$Q_s = A_a \cdot DNI \tag{29}$$

where η_{el} is the average electrical efficiency of the grid which takes values close to 33% [10]. A_a is the collector's aperture area.

4. Grid independence test and model validation

4.1. Grid system and independence test

To eliminate the influence of the grid number on the numerical results, grid independence test has been conducted with four grid systems when $T_{in,oil} = 500$ K, $\beta = 120°$ and $\lambda_{innertube} = 0.4$ W/(m·K). Grid system and the results of the grid independence test are presented in Fig. 3. It is observed that the relative variations for Nu, f, T_{max} and heat loss are limited within ±0.2% when the grid number increases from 555204 to 1628380. To balance the calculation time

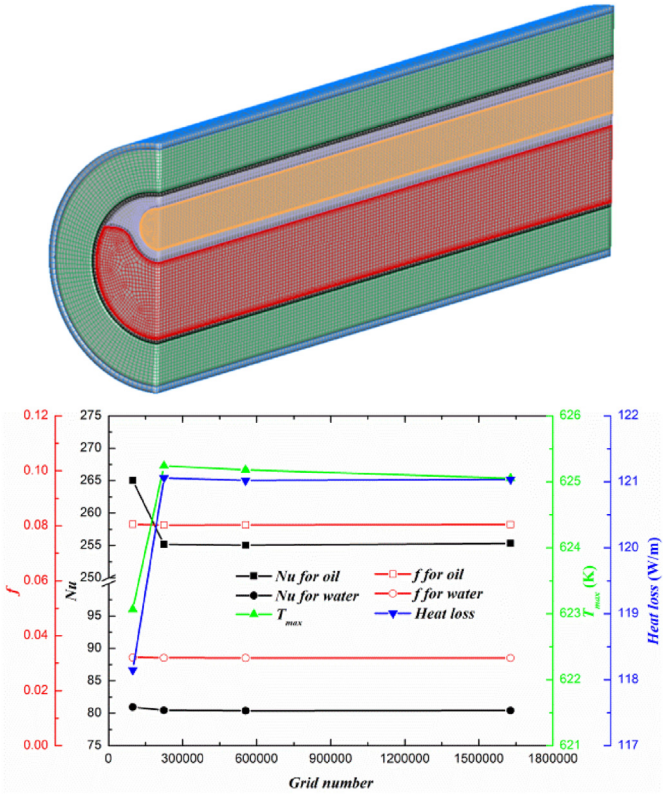

Fig. 3. Grid system and independence test.

and accuracy, the grid system with 555204 cells was selected for the numerical simulation later.

4.2. Model validation

In this study, the Gnielinski correlation for *Nu* and the Petukhov's correlation [51] for *f* under turbulent flow regime, which are expressed as Eqs. (30) and (31), were applied to verify the accuracy of the CFD model on calculating the heat transfer and flow resistance. Firstly, the heat transfer and flow characteristics of the oil flow in the CPTR were validated. The comparisons of *Nu* and *f* for the oil between the numerical results and correlations are demonstrated in Fig. 4 (a). It is observed that the relative differences of the *Nu* and *f* for the oil in CPTR are limited within ±4.6% and 3.6%, respectively. Then, the flow and heat transfer performance of the water in the inner tube of the NPTR were also verified. Fig. 4 (b) illustrates the comparisons of *Nu* and *f* between the calculating results and values from correlations. It can be found that the results in this study agree well with the values calculated by the correlations, as the relative differences of *Nu* and *f* for the water flow in the inner tube are limited within ±4.6% and 3.6%, respectively. These indicate that the developed CFD model is reliable.

$$Nu = \frac{(f/8)(\mathrm{Re}-1000)\mathrm{Pr}}{1+12.7(f/8)^{0.5}\left(\mathrm{Pr}^{2/3}-1\right)}\left[1+\left(\frac{d}{L}\right)^{2/3}\right] \tag{30}$$

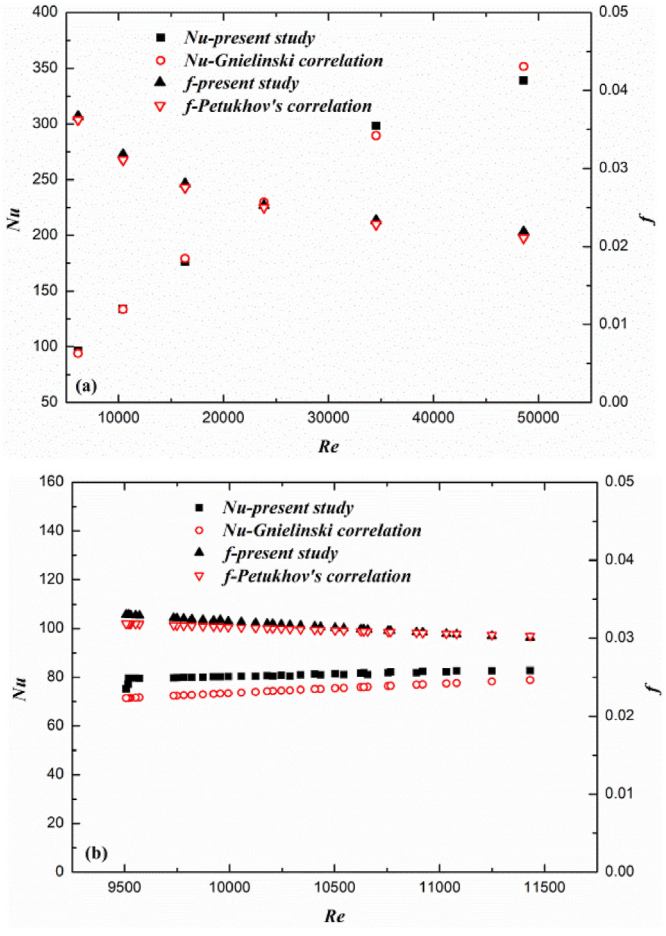

Fig. 4. Comparisons of *Nu* and *f* between the numerical results and the correlations: (a) oil in the CPTR; (b) water in the inner tube of NPTR.

$$f = (0.790\ln\mathrm{Re} - 1.64)^{-2} \tag{31}$$

To further validate the accuracy of the model, the simulation under the same operating parameters (as listed in Table 2) of the experiments from Dudley et al. [52], was conducted. The comparisons of temperature gain and heat collecting efficiency of a CPTR between the experimental data from Dudley et al. and the numerical results are illustrated in Fig. 5. It is seen that the numerical results show good agreement with the experimental data with the relative differences of temperature gain and heat collecting efficiency being limited in ±3.3% and ±1.9%. Therefore, the CFD model developed in this study has a reliable accuracy.

5. Results and discussion

5.1. Effects of inner tube and the central angle of the wing-like fringe

The wing-like fringe can prevent the HT-HTF from directly contacting the upper half of absorber inner surface. Thus, the central angle of the wing-like fringe has a significant influence on the performance of the NPTR. And its effects on the thermal-hydraulic and heat collecting performance are discussed when DNI = 1000 W/m^2 and $\lambda_{innertube}$ = 0.4 W/(m·K).

5.1.1. Distributions of velocity, temperature and heat flux

Figs. 6 and 7 present the velocity and temperature contours of the CPTR and NPTR with different β at the cross-section of z = 3.9 m and $T_{in,oil}$ = 500 K, respectively. It can be observed in Fig. 6 that the velocities of the LT-HTF in the inner tube of NPTRs are almost the same, as the cross-sectional areas of the LT-HTF are constant. However, the velocities of the HT-HTF in NPTRs are apparently higher than that of the CPTR, and the velocity increases with the increasing β. It is because compared to CPTR, the cross-sectional areas of HT-HTF in NPTRs are significantly reduced and the cross-sectional area decreases as the β increases. Moreover, the velocity gradients of HT-HTF near the absorber inner surface in NPTRs are dramatically aggrandized when compared to CPTR. This is beneficial to enhance the convective heat transfer between HT-HTF and absorber inner surface. As a result, it can be seen in Fig. 7 that the temperatures of the lower part of absorber in NPTRs are much lower than that of the CPTR. And the temperature on the lower part of absorber in NPTRs decreases with the increase of β. In addition, from Fig. 7, it is clear that the temperatures on the upper part of absorber in NPTRs are significantly reduced to even lower than the temperature of HT-HTF when compared to the CPTR. This is because the small heat flux on the upper part of absorber, where is illuminated by direct irradiance, is quickly taken away by the LT-HTF.

Fig. 8 (a) and (b) present the circumferential temperature and outward heat flux distributions on the absorber outer surfaces of PTRs under $T_{in,oil}$ = 500 K, respectively. From Fig. 8 (a), it is observed that the temperatures on the absorber outer surfaces of all NPTRs are significantly lower than that of the CPTR on the entire circumference. Moreover, it can be seen that in the area when $-90° < \theta < -30°$, the outer surface temperatures of absorbers in NPTRs decrease with the increase of β. This is because the velocity of HT-HTF is enlarged (as shown in Fig. 6) and the convective heat transfer in this area is enhanced as the β increases. In the area with $-30° < \theta < 90°$, the outer surface temperatures of absorbers in NPTRs decrease first ($\beta < 180°$) and then increase ($\beta > 180°$) with the increasing β. It is because in the area with $0° < \theta < 90°$ where is illuminated by direct irradiance, only a very low local heat flux transformed from solar irradiance is loaded, while in the area

Table 2
Operating parameters of Dudley's experiment.

Case	1	2	3	4	5	6	7	8
DNI(W/m^2)	933.7	968.2	982.3	909.5	937.9	880.6	920.9	903.2
Wind speed(m/s)	2.6	3.7	2.5	3.3	1.0	2.9	2.6	4.2
Air temperature (°C)	21.2	22.4	24.3	26.2	28.8	27.5	29.5	31.1
Flow rate (L/min)	47.70	47.78	49.10	54.70	55.50	55.60	56.80	56.30
$T_{in,oil}$ (°C)	102.2	151.0	197.5	250.7	297.8	299.0	379.5	355.9

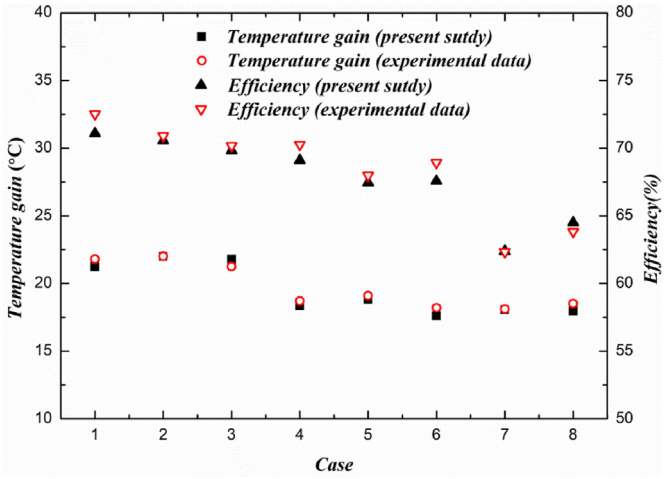

Fig. 5. Validation with experimental data from Dudley et al. [52].

with $-90° < \theta < 0°$ where is illuminated by concentrated irradiance, an extremely high local heat flux is loaded, as shown in Fig. 1 (d). When the $\beta > 180°$ (for example $\beta = 210°$), the high local heat flux from solar irradiance in the area with $-15° < \theta < 0°$ cannot be quickly taken away by the HT-HTF because the heat transfer from to the HT-HTF is obstructed by the wing-like fringe of the inner tube. Especially, in the area with about $10° < \theta < 90°$, the outer surface local temperatures of absorbers in NPTRs is much lower than the inlet temperature of HT-HTF (oil), while this local temperature of CPTR is close to the inlet temperature of HT-HTF. In addition, the area where the local temperature is lower than the inlet temperature of HT-HTF increases as the increase of β (When the $\beta < 180°$). The reason for this phenomenon is that the inner tube and the wing-like fringe can prevent the HT-HTF from directly contacting the upper part of absorber and the low local heat flux from solar irradiance can be taken away by the LT-HTF in the inner tube. From Fig. 8 (b), it can be viewed that the local outward heat flux on the absorber outer surfaces of all NPTRs are significantly lower than that of the CPTR on the entire circumference. Moreover, the variation trends of the local outward heat flux with θ and β are similar to the local temperature.

5.1.2. Heat transfer and flow resistance

The effects of β on the heat transfer and flow resistance of the HT-HTF under different inlet temperature of thermal oil ($T_{in,oil}$) are presented in Fig. 9 (a) and (b), respectively. It can be observed in Fig. 9 (a) that the heat transfer coefficients between the HT-HTF and

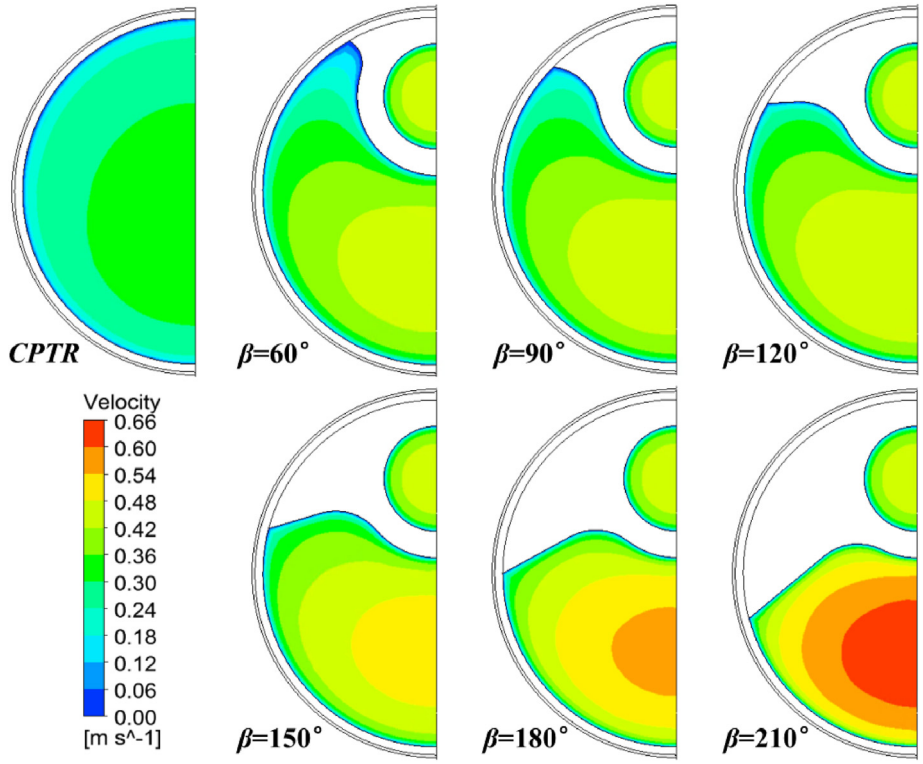

Fig. 6. Velocity distributions of the CPTR and NPTR with different β at the cross-section of $z = 3.9$ m.

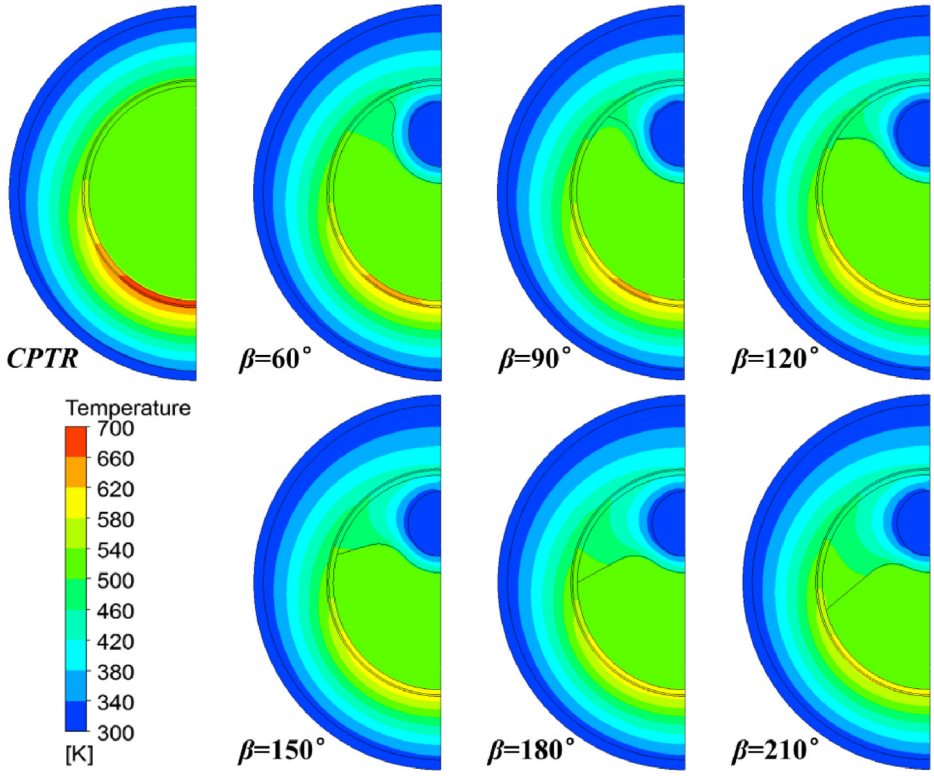

Fig. 7. Temperatures of the CPTR and NPTR with different β at the cross-section of $z = 3.9$ m.

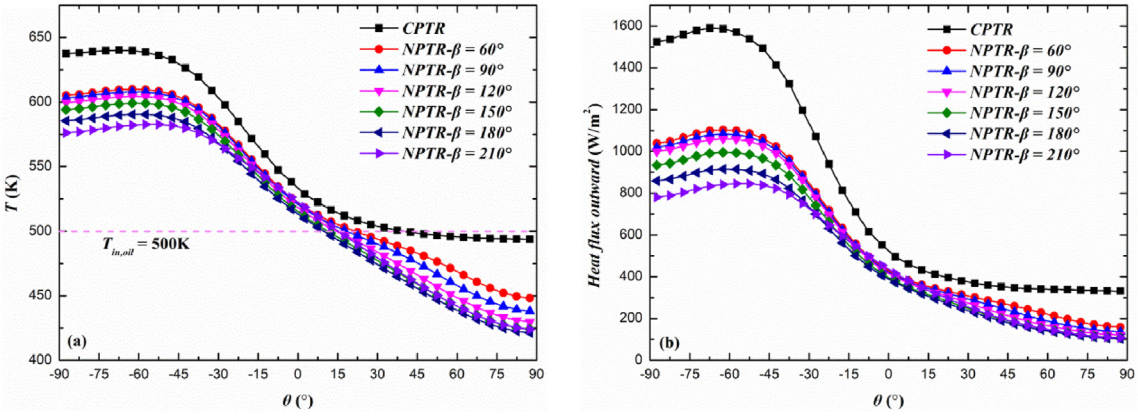

Fig. 8. Circumferential temperature and heat flux distributions on the outer surfaces of absorbers at $T_{in,oil} = 500$ K.

absorber inner surface of the NPTRs are enhanced to 1.37–1.89 times that of the CPTR. Furthermore, the heat transfer enhancement ratio (Nu/Nu_0) increases with the increasing β and decreases first then increases as $T_{in,oil}$ increases. Meanwhile, the flow resistances of the HT-HTF in NPTRs are also increased to 2.47–5.71 times that of the CPTR. And the flow resistance increase ratio (f/f_0) increases with the increasing β and decreases as $T_{in,oil}$ increases. Fig. 10 presents the variation of pumping work with β and $T_{in,oil}$. For the NPTRs as shown in Fig. 10 (a), the pumping work of the HT-HTF ($W_{p,\ oil}$) and LT-HTF ($W_{p,\ water}$) both increase with the increasing β. As the $T_{in,oil}$ increases, the $W_{p,\ oil}$ and $W_{p,\ water}$ show opposite trends, in which the former increases and the latter decreases. From Fig. 10 (b), it is clear that the total pumping work of the NPTRs (W_p) shows similar trends as the $W_{p,\ oil}$. It is because the $W_{p,\ oil}$ is much higher than the $W_{p,\ water}$ and dominates the pumping work. Furthermore, compared to the CPTR, the total pumping work of the NPTRs is increased by about 0.25–0.56 W.

5.1.3. Heat collecting performance

The variations of heat loss and efficiency with the β and $T_{in,oil}$ when DNI = 1000 W/m^2 are displayed in Fig. 11 (a) and (b), respectively. Firstly, for each PTR, the heat loss increases with the increasing $T_{in,oil}$ as shown in Fig. 11 (a). This is because the temperature difference between the absorber and the environment raises as the $T_{in,oil}$ increases. Furthermore, it can be viewed that the heat losses of NPTRs are apparently lower than that of the CPTR and descend with the increasing β due to the declining local temperature and outward heat flux on the absorber outer surface as shown in Fig. 8. As a result, it can be seen in Fig. 11 that the efficiency and heat loss show opposite trends because that the increase of heat

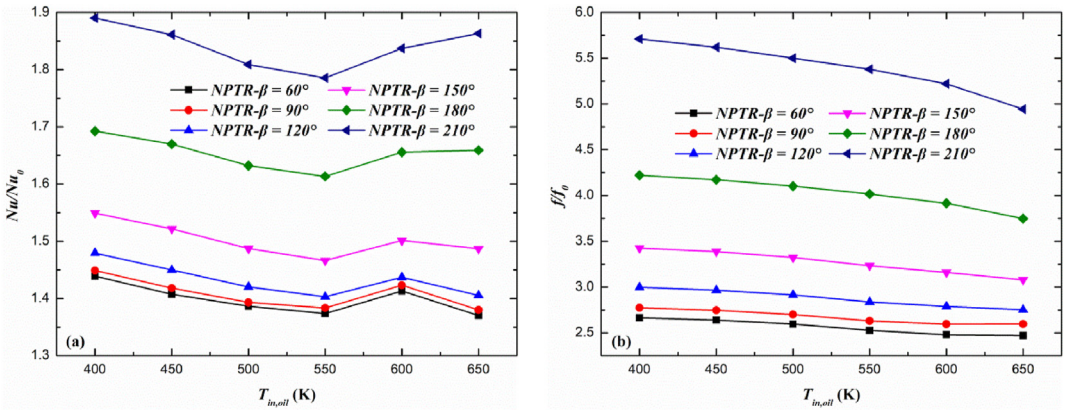

Fig. 9. Effects of β on the thermos-hydraulic performance of HT-HTF (thermal oil): (a) the heat transfer enhancement ratio (Nu/Nu_0); (b) the flow resistance increase ratio (f/f_0).

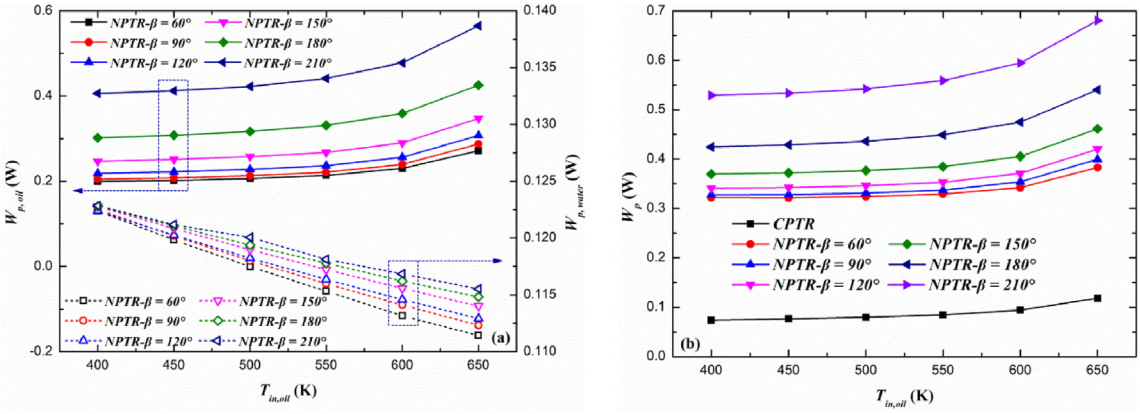

Fig. 10. The pumping work of CPTR and NPTRs at different β and $T_{in,oil}$.

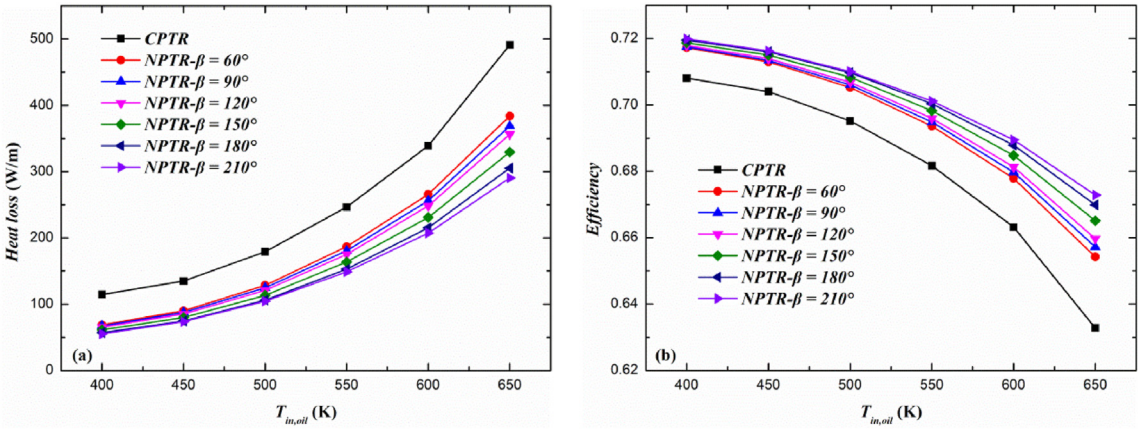

Fig. 11. Effects of β on the heat loss and efficiency of PTRs under different $T_{in,oil}$ when DNI = 1000W/m^2.

loss means the decrease of heat collecting efficiency and vice versa.

As the apportion of collecting heat in HT-HTF (oil) and LT-HTF (water) is an important characteristic of the cascade heat collection system, Fig. 12 (a) presents the proportions of oil and water heat gains in the total input solar energy under different β and $T_{in,oil}$. Firstly, it is clear that as the $T_{in,oil}$ increases, the proportion of oil heat gain decreases from 63.8% to 32.9% while the proportion of water heat gain increases from 8.2% to 32.5% due to the rising temperature difference and heat exchanger between the oil and water. Moreover, at the identical $T_{in,oil}$, the proportion of oil heat gain increases with the raising β, while the proportion of water heat gain decreases at the same time. It is because that as the β increases, the equivalent wall thickness of the inner tube increases and thus the heat transfer resistance between oil and water increases. The temperature gain of the HTFs represents the improvement degree of thermal quality in HTFs. Fig. 12 (b) presents the temperature gains of oil and water under different β and $T_{in,oil}$. It is observed that the temperature gains show the similar trends to proportions of

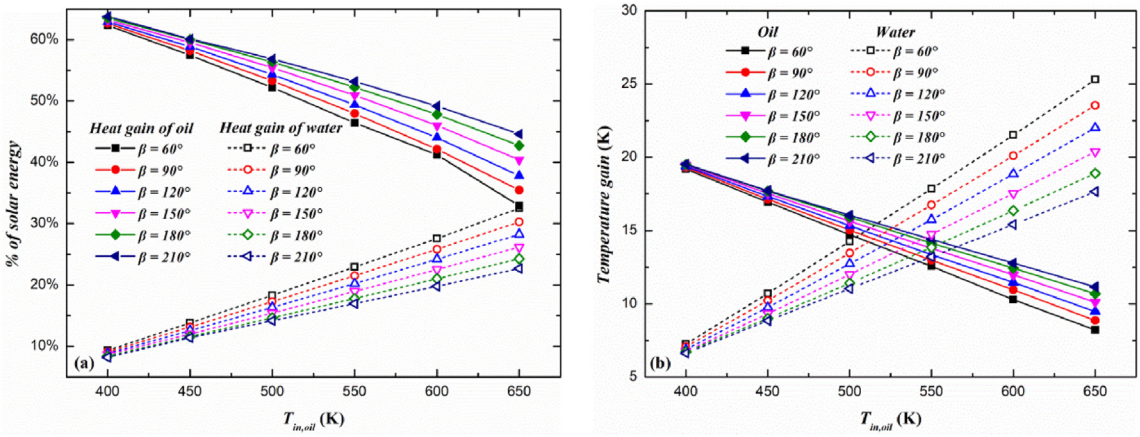

Fig. 12. Heat gains and temperature gains of HT-HTF and LT-HTF under different β and $T_{in,oil}$ when DNI = 1000W/m^2.

heat gains. In addition, the temperature gains of oil and water are ranged in 8.2–19.2 K and 6.6–25.3 K.

In addition, comprehensively considering the temperature distribution of absorber, heat transfer coefficient, total pumping work and overall efficiency of NPTR, the NPTR with $\beta = 180°$ is recommended as the optimal design and is selected to investigated the effects of thermal conductivity of the inner tube and direct normal irradiances below.

5.2. Effects of thermal conductivity of the inner tube

Although the thermal conductivity of the inner tube ($\lambda_{innertube}$) has no effect on the flow states of HTFs, it should have a great influence on the heat exchange between water and oil as well as heat transfer between water and the upper part of absorber. Thus, the effects of $\lambda_{innertube}$ are investigated under different $T_{in,oil}$ when $\beta = 180°$ and DNI = 1000 W/m^2. Fig. 13 displays the variations of the absorber maximum and minimum temperatures in NPTRs along the $\lambda_{innertube}$ under different $T_{in,oil}$. It is observed that at a certain $\lambda_{innertube}$, both the maximum and minimum temperatures of absorber in NPTRs increase with the raising $T_{in,oil}$. Moreover, as the $\lambda_{innertube}$ increases, the maximum temperature of absorber remains basically unchanged, while the minimum temperature of absorber is obviously reduced. It is because a large $\lambda_{innertube}$ is beneficial to the heat transfer between the water and upper part of absorber so as to reduce the local temperature of local in this area, while the $\lambda_{innertube}$ hardly affects the flow of oil as well as the local temperature at lower part of absorber.

Fig. 14 presents the effects of $\lambda_{innertube}$ on the heat loss and efficiency of NPTRs under different $T_{in,oil}$. It can be seen that the heat loss reduces with the increasing $\lambda_{innertube}$ due to the decreasing of temperature at upper part of absorber. Furthermore, the heat loss is more sensitive to the $\lambda_{innertube}$ at higher $T_{in,oil}$. As a result, the heat collecting efficiency of NPTRs increases with the raising $\lambda_{innertube}$. Moreover, the improvement in efficiency with the increase of $\lambda_{innertube}$ is more obvious at high $T_{in,oil}$.

The proportions of oil and water heat gains in the total input solar energy under different $\lambda_{innertube}$ and $T_{in,oil}$ are displayed in Fig. 15 (a). It is clear that the proportion of oil heat gain decreases with both the increasing $\lambda_{innertube}$ and $T_{in,oil}$, while the proportion of water heat gain shows the opposite trends. It is because that as the $\lambda_{innertube}$ or $T_{in,oil}$ increases, the heat transfer resistance between the oil and water decreases or the temperature difference between the oil and water increases. Fig. 15 (b) presents the temperature gains of oil and water under different $\lambda_{innertube}$ and $T_{in,oil}$. It can be viewed that the temperature gains of oil and water show the similar trends to those of the heat gains of oil and water.

5.3. Performance under different direct normal irradiances

Since the direct normal irradiance (DNI) varies greatly at different times of the day or under different weather, it is necessary to evaluate the performance of the NPTR at all possible conditions. In this study, the performance of NPTR with $\beta = 180°$ and

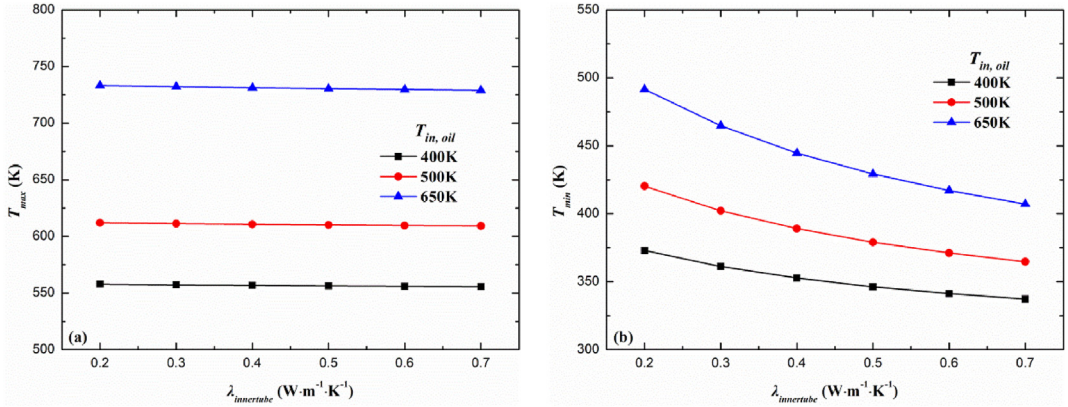

Fig. 13. Variations of absorber maximum and minimum temperatures in the NPTRs along with $\lambda_{innertube}$.

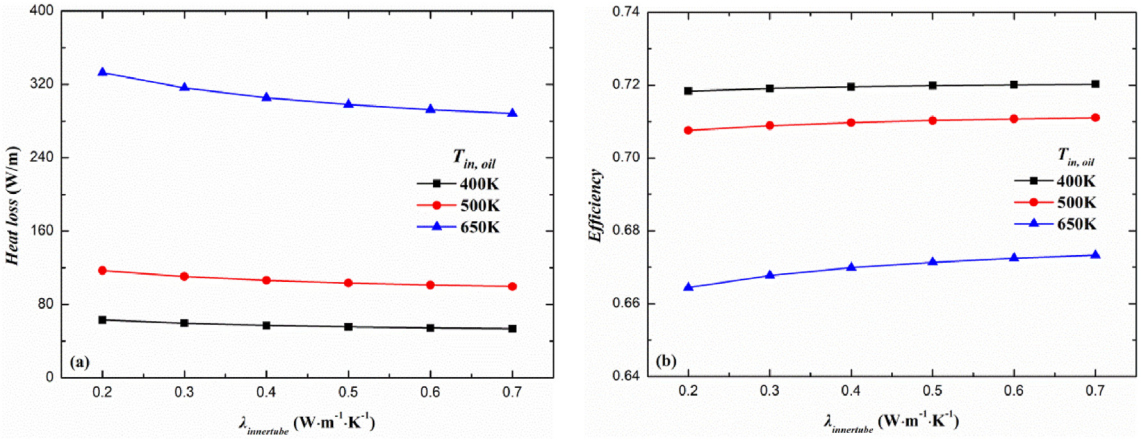

Fig. 14. Effects of thermal conductivity of inner tube on the heat loss and efficiency of PTRs when $\beta = 180°$ and DNI = 1000W/m^2.

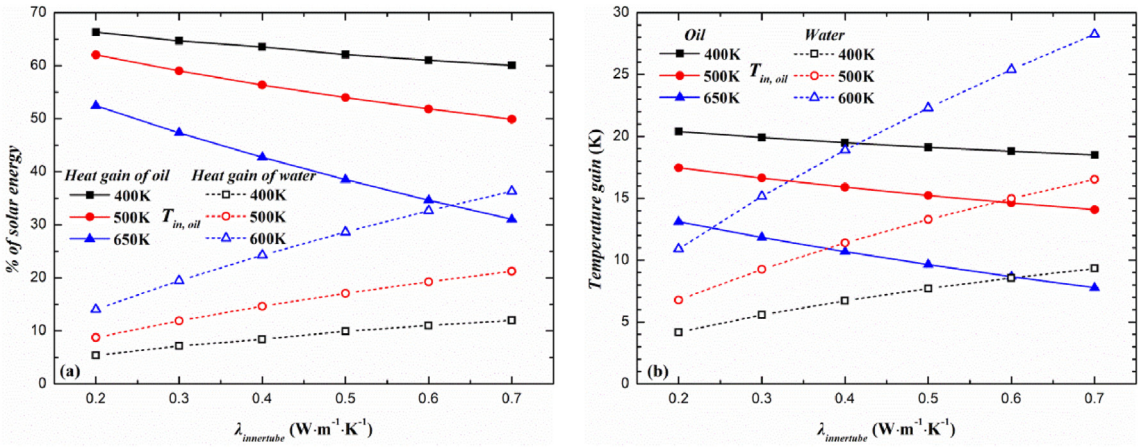

Fig. 15. Heat gains and temperature gains of HT-HTF and LT-HTF under different $\lambda_{innertube}$ and $T_{in,oil}$ when DNI = 1000W/m^2.

$\lambda_{innertube} = 0.4$ W/(m·K) is evaluated under different $T_{in,oil}$ and DNI. Moreover, the comparison of the performance between the NPTR and CPTR at different conditions is also discussed.

Fig. 16 (a) presents the heat losses of the NPTR and CPTR under different $T_{in,oil}$ and DNI. It is found that both the heat losses of the NPTR and CPTR at each $T_{in,oil}$ increase with the increasing DNI due to the rising temperature of absorber. And the increase rates of heat losses raise with the increase of DNI. In addition, the heat loss of the NPTR increases more gently with the raising DNI than that of the CPTR. Moreover, the heat loss of the NPTR is much lower than that of CPTR under all conditions. And compared to the CPTR, the reduction in heat loss of the NPTR is ranged in 9.2–185.8 W/m with the relative reduction of heat loss is located in 33.1%–50.1%. The overall efficiencies of the NPTR and CPTR under different $T_{in,oil}$ and DNI are displayed in Fig. 16 (b). It is observed that when $T_{in,oil} >$ 450 K, the efficiencies of NPTR and CPTR raise with the increase of DNI, while they increase first and then decrease gently with the increasing DNI when $T_{in,oil} \leq 450$ K. This is because at low $T_{in,oil}$ and large DNI, the relative increase rate of heat loss is greater than that of DNI, while at high $T_{in,oil}$ or small DNI, the relative increase rate of heat loss is less than that of DNI. Furthermore, the overall efficiency of NPTR is obviously higher than that of the CPTR under all the studied conditions. Compared to the CPTR, the overall efficiency of NPTR is improved by 0.61%–7.67%. And the improvement in overall efficiency increases with the decreasing DNI and increasing $T_{in,oil}$.

Fig. 17 (a) demonstrates the proportions of oil and water heat gains in the total input solar energy under different DNI and $T_{in,oil}$. It is clear that at an identical $T_{in,oil}$, the proportion of oil heat gain increases with the increase of DNI, while the proportion of water heat gain decreases with the increasing DNI. The reason for this trend is that as the DNI increases, the heat gain of water increases very gently and is almost unchanged, while the heat gain of the oil increases more sharply than that of the total input solar energy. Moreover, at a certain DNI, the heat gain of water increases while the heat gain of oil decreases with the increase of $T_{in,oil}$ due to more heat being exchanged from oil to water at a higher $T_{in,oil}$. Especially, at the conditions with high $T_{in,oil}$ (>600 K) and small DNI (<400 W/m^2), the proportion of oil heat gain is negative. It is because under these conditions, the heat exchange from oil to water is larger than the heat gain of oil from the concentrated solar irradiance. The proportions of oil and water heat gains in the total input solar energy are ranged in −18.8–63.5% and 8.39–77.6% when DNI = 300–1000 W/m^2 and $T_{in,oil} = 400$–650 K, respectively. The temperature gains of oil and water are presented in Fig. 17 (b). It is viewed that the temperature gain of oil increases sharply with the rising DNI, while the temperature gain of water increases very gently. And at a certain DNI, temperature gain of oil decreases with the increasing $T_{in,oil}$, while the temperature gain of water shows opposite trend. The temperature gains of oil and water are ranged in −1.4–19.5 K and 5.4–18.8 K, respectively. It is concluded that the heat gain of water comes mainly from heat exchange with oil. Thus the temperature gain of water is much more sensitive to $T_{in,oil}$ than DNI.

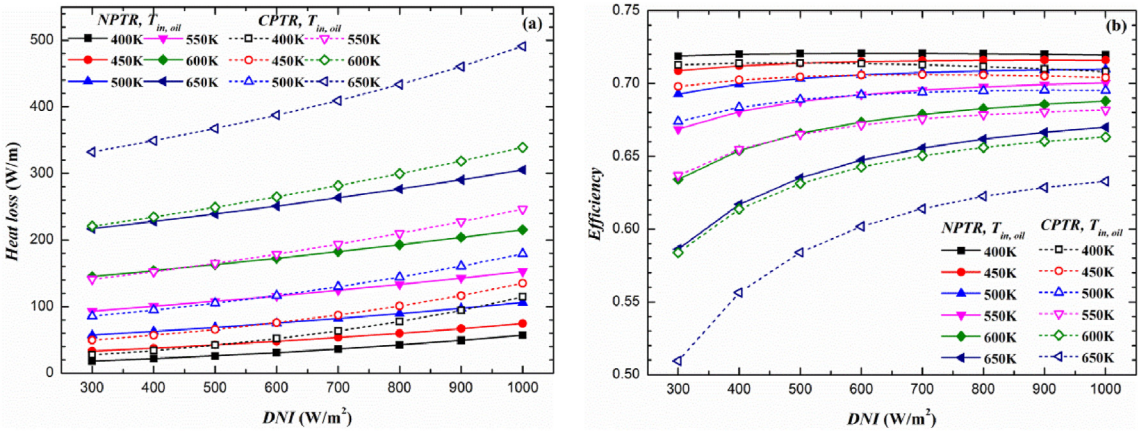

Fig. 16. Heat loss and overall efficiency of the CPTR and NPTR under different $T_{in,oil}$ and DNI.

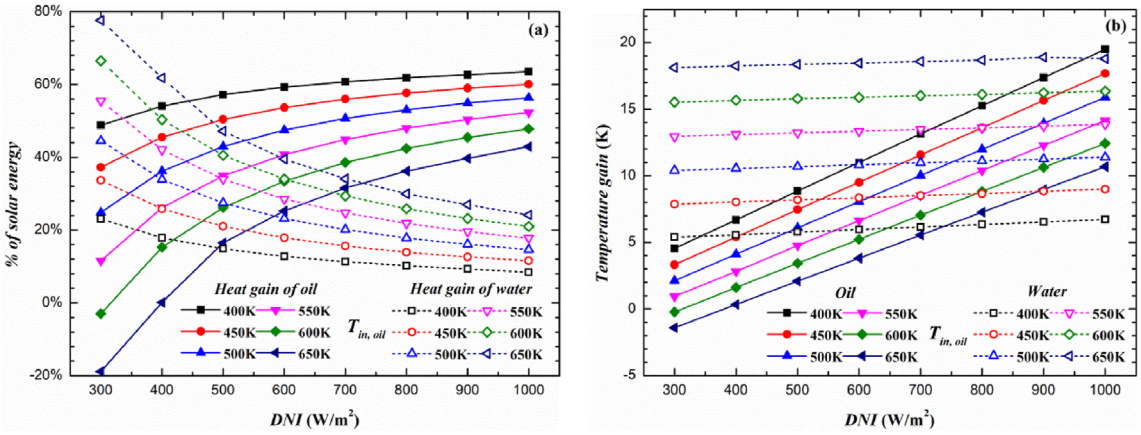

Fig. 17. Heat gains and temperature gains of HT-HTF and LT-HTF under different $T_{in,oil}$ and DNI.

6. Conclusions

In this study, a novel parabolic trough receiver integrated with an inner tube and wing-like fringe for solar cascade heat collection was proposed to improve heat collecting efficiency and provide different grades of thermal energy. And a three-dimensional computational fluid dynamics (CFD) model was established to study the performance of the NPTR. The main conclusions drawn in this work are as follow.

(1) Effects of inner tube and central angle of the wing-like fringe (β) under different inlet temperature ($T_{in,oil}$) of HT-HTF (oil) are investigated. Firstly, compared to CPTR, the cross-sectional area of oil in NPTR is significantly compressed and the velocity of oil in NPTR is apparently enlarged. Thus, the heat transfer between oil and absorber is enhanced by 37%–89% accompanied by 147%–471% increase in flow resistance of oil and the total pumping work is increased by about 0.25–0.56 W. Furthermore, the absorber temperature and heat loss of the NPTR is dramatically reduced, and thus the NPTR obtains effective improvement in overall efficiency. Second, the velocity of oil, heat transfer coefficient between oil and absorber, flow resistance and the total pumping work all increase with the increasing β. Both local temperature and local outward heat flux on lower part of the absorber outer surfaces decrease with the increase of β, while the local temperature and local outward heat flux on upper part of the absorber outer surfaces decrease first (when $\beta < 180°$) and then increase (when $\beta > 180°$) with the rising β. Moreover, as the β increases, the heat loss is reduced and thus the overall efficiency is improved. The proportion of oil heat gain and temperature gain increase while the proportion of water heat gain and temperature gain decrease with the raising β. In addition, considering that the local outward heat flux on upper part of the absorber outer surfaces reaches to the minimum at $\beta = 180°$, the NPTR with $\beta = 180°$ is recommended as the suggested design.

(2) The effects of thermal conductivity of the inner tube ($\lambda_{innertube}$) are also studied in this study. It is indicated that the local temperature (minimum temperature) on the upper part of absorber decreases as the $\lambda_{innertube}$ increases. Thus, the heat loss is slightly reduced and the overall efficiency is consequently improved with the increase of $\lambda_{innertube}$. Especially, the $\lambda_{innertube}$ has a great influence on the heat exchange between the oil and water. Thus, the heat gain and temperature gain of oil decrease sharply as the $\lambda_{innertube}$ increases, while the heat gain and temperature gain of oil increase sharply at the same time.

(3) Performance of the suggested NPTR with $\beta = 180°$ and $\lambda_{innertube} = 0.4$ W/(m·K) under different operating conditions (DNI = 300–1000 W/m^2 and $T_{in,oil}$ = 400–650 K) are evaluated. It is found that in comparison to the CPTR, the NPTR can effectively reduce heat loss by 33.1–50.1% (9.2–185.8 W/m). And thus the overall efficiency of NPTR is improved by

0.61%–7.67%. Moreover, the proportion of oil heat gain increases with the increasing DNI and decreasing $T_{in,oil}$. While the proportion of water heat gain increases very gently with the increasing DNI and decreases with the decreasing $T_{in,oil}$. The proportions of oil and water heat gains in the total input solar energy are ranged in −18.8–63.5% and 8.39–77.6%, respectively. As a result, the temperature gains of oil and water are ranged in −1.4–19.5 K and 5.4–18.8 K, respectively.

In summary, the NPTR with an inner tube and wing-like fringe is able to provide different grades of thermal energy for electricity and fresh water production at the same time. Moreover, the NPTR can obtain higher overall thermal efficiency than CPTR under the typical broad extents of operating conditions, and it has a good application potential in the comprehensive utilization of solar thermal energy.

CRediT authorship contribution statement

Peng Liu: Conceptualization, Methodology, Validation, Formal analysis, Investigation, Data curation, Writing - original draft, Writing - review & editing. **Zhimin Dong:** Methodology, Validation, Formal analysis, Investigation, Writing - review & editing. **Hui Xiao:** Methodology, Formal analysis, Investigation, Data curation, Writing - review & editing. **Zhichun Liu:** Resources, Supervision, Project administration. **Wei Liu:** Conceptualization, Resources, Supervision, Project administration, Funding acquisition.

Declaration of competing interest

To the best of our knowledge and belief, neither I nor any co-authors have any possible conflict of interest.

Acknowledgment

The work was supported by the National Natural Science Foundation of China (Grant No. 51736004).

References

[1] W. Fuqiang, C. Ziming, T. Jianyu, Y. Yuan, S. Yong, L. Linhua, Progress in concentrated solar power technology with parabolic trough collector system: a comprehensive review, Renew. Sustain. Energy Rev. 79 (2017) 1314–1328.
[2] A.J. Abdulhamed, N.M. Adam, M.Z.A. Ab-Kadir, A.A. Hairuddin, Review of solar parabolic-trough collector geometrical and thermal analyses, performance, and applications, Renew. Sustain. Energy Rev. 91 (2018) 822–831.
[3] İ.H. Yılmaz, A. Mwesigye, Modeling, simulation and performance analysis of parabolic trough solar collectors: a comprehensive review, Appl. Energy 225 (2018) 135–174.
[4] G. Kumaresan, P. Sudhakar, R. Santosh, R. Velraj, Experimental and numerical studies of thermal performance enhancement in the receiver part of solar parabolic trough collectors, Renew. Sustain. Energy Rev. 77 (2017) 1363–1374.
[5] M.T. Islam, N. Huda, A.B. Abdullah, R. Saidur, A comprehensive review of state-of-the-art concentrating solar power (CSP) technologies: current status and research trends, Renew. Sustain. Energy Rev. 91 (2018) 987–1018.
[6] F.E. Ahmed, R. Hashaikeh, N. Hilal, Solar powered desalination – technology, energy and future outlook, Desalination 453 (2019) 54–76.
[7] R. Long, Z. Kuang, Z. Liu, W. Liu, Ionic thermal up-diffusion in nanofluidic salinity-gradient energy harvesting, Natl. Sci. Rev. 6 (6) (2019) 1266–1273.
[8] E. Vengadesan, R. Senthil, A review on recent development of thermal performance enhancement methods of flat plate solar water heater, Sol. Energy 206 (2020) 935–961.
[9] Y.-L. He, Y. Qiu, K. Wang, F. Yuan, W.-Q. Wang, M.-J. Li, J.-Q. Guo, Perspective of concentrating solar power, Energy 198 (2020) 117373.
[10] E. Bellos, C. Tzivanidis, Alternative designs of parabolic trough solar collectors, Prog. Energy Combust. Sci. 71 (2019) 81–117.
[11] G.K. Manikandan, S. Iniyan, R. Goic, Enhancing the optical and thermal efficiency of a parabolic trough collector – a review, Appl. Energy 235 (2019) 1524–1540.
[12] Q. Wang, H. Yang, X. Huang, J. Li, G. Pei, Numerical investigation and experimental validation of the impacts of an inner radiation shield on parabolic trough solar receivers, Appl. Therm. Eng. 132 (2018) 381–392.
[13] E. Bellos, C. Tzivanidis, Enhancing the performance of a parabolic trough collector with combined thermal and optical techniques, Appl. Therm. Eng. 164 (2020) 114496.
[14] Q. Li, Y. Zhang, Z.-X. Wen, Y. Qiu, An evacuated receiver partially insulated by a solar transparent aerogel for parabolic trough collector, Energy Convers. Manag. 214 (2020) 112911.
[15] Y. Qiu, Y. Zhang, Q. Li, Y. Xu, Z.-X. Wen, A novel parabolic trough receiver enhanced by integrating a transparent aerogel and wing-like mirrors, Appl. Energy 279 (2020) 115810.
[16] H. Yang, Q. Wang, S. Zhong, T.H. Kwan, J. Feng, J. Cao, G. Pei, Spectral-spatial design and coupling analysis of the parabolic trough receiver, Appl. Energy 264 (2020) 114692.
[17] Q. Wang, H. Yang, M. Hu, J. Cao, G. Pei, H. Yang, Optimization strategies and verifications of negative thermal-flux region occurring in parabolic trough solar receiver, J. Clean. Prod. 278 (2021) 123407.
[18] Y. Qiu, M. Xu, Q. Li, Y. Xu, J. Wang, A novel evacuated receiver improved by a spectral-selective glass cover and rabbit-ear mirrors for parabolic trough collector, Energy Convers. Manag. 227 (2021) 113589.
[19] W. Liu, P. Liu, Z.M. Dong, K. Yang, Z.C. Liu, A study on the multi-field synergy principle of convective heat and mass transfer enhancement, Int. J. Heat Mass Tran. 134 (2019) 722–734.
[20] W. Liu, P. Liu, J.B. Wang, N.B. Zheng, Z.C. Liu, Exergy destruction minimization: a principle to convective heat transfer enhancement, Int. J. Heat Mass Tran. 122 (2018) 11–21.
[21] M. Gupta, V. Singh, R. Kumar, Z. Said, A review on thermophysical properties of nanofluids and heat transfer applications, Renew. Sustain. Energy Rev. 74 (2017) 638–670.
[22] S.K. Verma, A.K. Tiwari, Progress of nanofluid application in solar collectors: a review, Energy Convers. Manag. 100 (2015) 324–346.
[23] H.M. Sandeep, U.C. Arunachala, Solar parabolic trough collectors: a review on heat transfer augmentation techniques, Renew. Sustain. Energy Rev. 69 (2017) 1218–1231.
[24] S. Akbarzadeh, M.S. Valipour, Heat transfer enhancement in parabolic trough collectors: a comprehensive review, Renew. Sustain. Energy Rev. 92 (2018) 198–218.
[25] O.A. Jaramillo, M. Borunda, K.M. Velazquez-Lucho, M. Robles, Parabolic trough solar collector for low enthalpy processes: an analysis of the efficiency enhancement by using twisted tape inserts, Renew. Energy 93 (2016) 125–141.
[26] X. Song, G. Dong, F. Gao, X. Diao, L. Zheng, F. Zhou, A numerical study of parabolic trough receiver with nonuniform heat flux and helical screw-tape inserts, Energy 77 (2014) 771–782.
[27] P. Liu, N. Zheng, Z. Liu, W. Liu, Thermal-hydraulic performance and entropy generation analysis of a parabolic trough receiver with conical strip inserts, Energy Convers. Manag. 179 (2019) 30–45.
[28] K.S. Reddy, K. Ravi Kumar, C.S. Ajay, Experimental investigation of porous disc enhanced receiver for solar parabolic trough collector, Renew. Energy 77 (2015) 308–319.
[29] C. Chang, A. Sciacovelli, Z. Wu, X. Li, Y. Li, M. Zhao, J. Deng, Z. Wang, Y. Ding, Enhanced heat transfer in a parabolic trough solar receiver by inserting rods and using molten salt as heat transfer fluid, Appl. Energy 220 (2018) 337–350.
[30] A. Mwesigye, T. Bello-Ochende, J.P. Meyer, Multi-objective and thermodynamic optimisation of a parabolic trough receiver with perforated plate inserts, Appl. Therm. Eng. 77 (2015) 42–56.
[31] P. Wang, D.Y. Liu, C. Xu, Numerical study of heat transfer enhancement in the receiver tube of direct steam generation with parabolic trough by inserting metal foams, Appl. Energy 102 (2013) 449–460.
[32] E. Bellos, C. Tzivanidis, I. Daniil, K.A. Antonopoulos, The impact of internal longitudinal fins in parabolic trough collectors operating with gases, Energy Convers. Manag. 135 (2017) 35–54.
[33] J. Muñoz, A. Abánades, Analysis of internal helically finned tubes for parabolic trough design by CFD tools, Appl. Energy 88 (11) (2011) 4139–4149.
[34] Z.D. Cheng, Y.L. He, F.Q. Cui, Numerical study of heat transfer enhancement by unilateral longitudinal vortex generators inside parabolic trough solar receivers, Int. J. Heat Mass Tran. 55 (21) (2012) 5631–5641.
[35] H. Xiao, P. Liu, Z. Liu, W. Liu, Performance analyses in parabolic trough collectors by inserting novel inclined curved-twisted baffles, Renew. Energy 165 (2021) 14–27.
[36] P. Liu, J. Lv, F. Shan, Z. Liu, W. Liu, Effects of rib arrangements on the performance of a parabolic trough receiver with ribbed absorber tube, Appl. Therm. Eng. 156 (2019) 1–13.
[37] W. Fuqiang, L. Qingzhi, H. Huaizhi, T. Jianyu, Parabolic trough receiver with corrugated tube for improving heat transfer and thermal deformation characteristics, Appl. Energy 164 (2016) 411–424.
[38] E. Bellos, C. Tzivanidis, D. Tsimpoukis, Thermal enhancement of parabolic trough collector with internally finned absorbers, Sol. Energy 157 (2017) 514–531.
[39] A. Omar, A. Nashed, Q. Li, G. Leslie, R.A. Taylor, Pathways for integrated concentrated solar power - desalination: A critical review, Renew. Sustain. Energy Rev. 119 (2020) 109609.
[40] H. Sharon, K.S. Reddy, A review of solar energy driven desalination technologies, Renew. Sustain. Energy Rev. 41 (2015) 1080–1118.
[41] Y. Zheng, K.B. Hatzell, Technoeconomic analysis of solar thermal desalination, Desalination 474 (2020) 114168.

[42] J.A. Andrés-Mañas, L. Roca, A. Ruiz-Aguirre, F.G. Acién, J.D. Gil, G. Zaragoza, Application of solar energy to seawater desalination in a pilot system based on vacuum multi-effect membrane distillation, Appl. Energy 258 (2020) 114068.
[43] J.H. Reif, W. Alhalabi, Solar-thermal powered desalination: its significant challenges and potential, Renew. Sustain. Energy Rev. 48 (2015) 152–165.
[44] P. Liu, Z. Dong, H. Xiao, Z. Liu, W. Liu, Thermal-hydraulic performance analysis of a novel parabolic trough receiver with double tube for solar cascade heat collection, Energy 219 (2021) 119566.
[45] X. Zhu, L. Zhu, J. Zhao, Wavy-tape insert designed for managing highly concentrated solar energy on absorber tube of parabolic trough receiver, Energy 141 (2017) 1146–1155.
[46] B. Nait-Ali, K. Haberko, H. Vesteghem, J. Absi, D.S. Smith, Preparation and thermal conductivity characterisation of highly porous ceramics: comparison between experimental results, analytical calculations and numerical simulations, J. Eur. Ceram. Soc. 27 (2) (2007) 1345–1350.
[47] A. Mwesigye, T. Bello-Ochende, J.P. Meyer, Heat transfer and thermodynamic performance of a parabolic trough receiver with centrally placed perforated plate inserts, Appl. Energy 136 (2014) 989–1003.
[48] Y.-L. He, J. Xiao, Z.-D. Cheng, Y.-B. Tao, A MCRT and FVM coupled simulation method for energy conversion process in parabolic trough solar collector, Renew. Energy 36 (3) (2011) 976–985.
[49] R. Forristall, Heat Transfer Analysis and Modeling of a Parabolic Trough Solar Receiver Implemented in Engineering Equation Solver, Technical, 2003. Report, NREL/TP-550-34169.
[50] S.C. Mullick, S.K. Nanda, An improved technique for computing the heat loss factor of a tubular absorber, Sol. Energy 42 (1) (1989) 1–7.
[51] P.D.W.F.P. Incropera, T.L. Bergman, A.S. Lavine, Fundamentals of Heat and Mass Transfer, sixth ed., John-Wiley & Sons, 2006.
[52] S.M. Dudley EV, J.G. Kolb, D. Kearney, SEGS LS2 Solar Collector-Test Results, Report of Sandia National Laboratories, 1994, pp. SAN94–1884.